EXPERIMENTAL DETERMINATION OF LITHIUM PARTITIONING BETWEEN CLINOPYROXENE AND MELT

A Thesis

Presented to the Faculty of the Graduate School

of Cornell University

In Partial Fulfillment of the Requirements for the Degree of

Master of Science

by

MEGAN FAIRCHILD

MAY 2023

© 2023 MEGAN FAIRCHILD

ABSTRACT

Planetary habitability is enabled by the transfer of volatile substances like H_2O from planetary interiors to surfaces during volcanic degassing, but fully degassed rocks will not retain a geochemical record of these processes. The element lithium (Li) is thought to behave moderately volatilely and may function as a proxy for H_2O in completely degassed systems, like Martian meteorites. Here we present new experimental measurements of Li partitioning between clinopyroxene and melts to examine if Li trends in Martian meteorites may be attributable to processes other than H_2O degassing. We find Li is moderately incompatible in clinopyroxene in both compositions and identify potential partitioning trends with temperature and pressure. We used the new data to model the concentration of Li in cpx during cooling. Our cooling model reproduces Li trends in Martian cpx, suggesting that previous hypotheses regarding H_2O in the Martian interior may need to be re-evaluated.

BIOGRAPHICAL SKETCH

Megan Fairchild grew up in Salt Lake City, Utah, where the natural landscapes fostered her love of rocks and later, the field of geology. She attended Westminster College of Salt Lake City for her Bachelor's degree, graduating in Geology and Honors in 2020. Megan continued her academic career at Cornell beginning in 2021 as a Sloan Fellow. She will graduate with her Master of Science May 2023.

Dedicated to the women in STEM who came before me.

ACKNOWLEDGMENTS

I would like to thank my advisor, Dr. Megan Holycross, first and foremost. Thank you for your never-ending patience and sound guidance through all of this. I've learned many lessons during our time together and appreciate the opportunity to have worked with her. Additionally, I would like to thank my other committee members, Matthew Pritchard and Esteban Gazel for their feedback and support.

Special thanks to Lyndsey Fisher, Jay Thomas, Dustin Trail, and Wriju Chowdhury for their time and assistance with the analytical work for this project. And a shoutout to Kyle Dayton and Brendan Garvey for their Iolite expertise.

Lastly, I would like to thank my family and friends for their support and encouragement. They have been critical to my success at Cornell.

TABLE OF CONTENTS

LIST OF FIGURES

LIST OF TABLES

LIST OF ABBREVIATIONS

1 LLE: Light Ion Lithophile Element

2 Li: Lithium

3 B: Boron

4 Cl: Chlorine

5 D: Partition Coefficient

6 Z: atomic number

7 g: gram

8 cm: centimeter

9 Cpx: Clinopyroxene

10 MORB: Mid-ocean ridge basalt

11 Atm: atmosphere

12 Ppm: parts per million

13 P: Pressure

14 T: temperature

15 t: time

16 hrs: hours

17 min: minutes

18 s: seconds

19 GPa: gigapascal

20 LA-ICP-MS: Laser ablation inductively coupled mass spectrometry

21 kV: kilovolt

nA: nano ampere

nm: nanometer

J: joules

Hz: hertz

n: number of analyses

SD: standard deviation from the mean

SE: standard error

BSE: Back-scatter Electron

Opx: orthopyroxene

Plag: Plagioclase

Grt: Garnet

Wo: Wollastonite component of cpx

En: Enstatite component of cpx

Fs: Ferrosilite component of cpx

LIST OF SYMBOLS

1 °C: degrees Celsius

2 µg/g: microgram per gram

3 Wt%: weight percent

4 µm: micrometer

5 ”: inch

6 1σ: one standard deviation

7 R^2: coefficient of determination

8 C_R: Concentration of element in the mineral

9 C_O: Initial concentration of element

PREFACE

Understanding the behavior of water and other volatile, or "easily vaporized", substances is key for deciphering planetary formation and evolution and determining how a planet can become habitable for complex life. The transfer of water from a planet's interior to its surface happens largely through volcanic degassing, where water and other volatiles, such as carbon dioxide, exsolve from the magma during ascent and are released at the surface as vapor or gas. This process is instrumental for the formation of a hydrosphere that is capable of supporting life. In addition, the formation and migration of volatile-carrying hydrothermal fluids is also important for the formation of ore deposits, which help sustain life and have economic importance for the human population. However, there are large gaps in our knowledge about the behavior of volatiles during magmatic processes, particularly because there is often no geochemical record left behind in systems that have lost all of their highly volatile elements such as CO_2 and H_2O. It may be possible to rectify these gaps in information by using other elements that mimic the behavior of highly volatile elements as a proxy.

It has been argued that the Light Lithophile Elements (LLEs; here, Li, and B) will degas during volcanic eruptions along with highly volatile species like H_2O (Webster et al. 1989; Berlo et al. 2004; Hervig et al. 2004; Iveson et al. 2019; Giuffrida et al. 2017; Neukampf et al. 2020), indicating that LLE abundances may be a viable proxy for water in systems where H_2O has fully degassed. Variations in the core-to-rim content of Li and B in terrestrial and Martian minerals has previously been interpreted

as the result of diffusion out of the crystal during degassing (McSween 2001; Beck et al. 2004; Giuffrida et al. 2007; Kent et al. 2007; Udry et al. 2016). Reliable partition coefficients, which quantitatively describe how elements preferentially separate into the melt, mineral, or fluid phase in measured experiments, e.g.,

$$D_{Li}^{mineral/melt} = \frac{Li\ in\ mineral}{Li\ in\ melt} \qquad (1)$$

are vital to understand the thermodynamic cause of these variations. However, the partitioning of Li and B in both mineral-melt and melt-fluid systems has been largely ignored in experimental work, especially in mafic systems, leaving a large gap in available information.

INTRODUCTION

1.1 Geochemical Background

Lithium (Li) (Z = 3) has been of growing interest to the scientific community in recent years, particularly as a critical element due to the growth of the clean energy movement and as an isotopic tracer of surface processes and crustal recycling. Lithium is the first element in the alkali metals group and the lightest of the alkali metals, with a density of 0.543 $g\ cm^{-3}$, the lowest of all the metals. Though the density of boron is significantly higher (2.46 $g\ cm^{-3}$), it also has a relatively low atomic mass. All LLEs are believed to be incompatible in most mineral phases (e.g., D<1; e.g., Brenan et al. 1998; Ottolini et al. 2009), as well as moderately volatile in silicic magmas (e.g., Webster et al. 1989), and thus they may be useful tracers of igneous differentiation and hydrothermal processes. For instance, the Bulk silicate Earth is estimated to contain 1.39 μg/g Li (Marschall et al. 2017) and the continental crust is estimated to contain 21 μg/g, suggesting Li was concentrated in the continental crust during differentiation and could effectively record partial melting processes in the mantle. Li and B are soluble in an aqueous phase at temperatures greater than 350° C (Seyfried et al. 1984), and it has been suggested their relatively high abundance in subduction zones rocks may result from the transfer of aqueous fluids from the slab to the arc mantle (Brennan et al. 1998).

In addition to tracing crustal differentiation and mass transfer throughout the subduction system, the LLE geochemistry of meteorites may provide insights into Martian volcanism and habitability. McSween et al. (2001) measured core-to-rim

decreases in the concentration of Li and B (reverse zoning) in clinopyroxenes (cpx) from the Shergotty meteorite. The reverse zoning of incompatible Li and B in cpx is opposite of what is expected from normal igneous differentiation. Consequently, McSween et al. (2001) argued that the reverse zoning of Li and B in cpx records the degassing of Martian magmas prior to eruption. This hypothesis implies that Li and B partitioned from cpx into a separate fluid or vapor phase as the magma decompressed during ascent to the Martian surface. The presence of an exsolved fluid/vapor phase at depth suggests that the initial water content of Martian magmas (estimated at 1.8 wt%, McSween et al. 2001) exceeded the measured solubility of H_2O in the melt during magma decompression. Following McSween et al. 2001, multiple studies (e.g., Lentz et al. 2001, Herd et al. 2004, Beck et al. 2004, Udry et al. 2016) characterized LLE zoning in pyroxenes in the Zagami, Shergotty, and NWA 480 meteorites. These studies all found the total or 'bulk' concentrations of Li and B are zoned in Zagami and Shergotty cpx. The Li isotope composition of cpx in NWA 480 are also zoned (e.g., Beck et al. 2004, Udry et al. 2016). Like McSween et al. 2001, these studies attributed the depletion of Li and B in pyroxene rims to magmatic degassing in the Martian mantle.

While the compositions of Martian meteorites suggest certain LLEs may be volatile at magmatic temperatures, the evidence from terrestrial systems is less clear. Edmonds (2015) measured the concentrations of LLEs in olivine-hosted melt inclusions from Kilauea, HI (a potential Martian analog) and found that Li and B partition only weakly into the vapor phase in basaltic magmas. Edmonds (2015) found that the vapor-melt partition coefficient of Li must be at least an order of magnitude

greater than measured at Kilauea to attribute the trends in Martian meteorites to degassing. If Li and B are not volatile at the conditions of basaltic magmatism in planetary interiors, then another unidentified phenomenon must be responsible for the reverse zoning of LLEs observed in Martian meteorites.

1.2 Previous experimental work

The hypothesis that Martian magmas were initially hydrous is critical for understanding the long-term history of water on the planet and determining whether its surface may have previously been able to support biological life. The validity of this hypothesis rests on the idea that Li and B will partition from mafic minerals and melts into a fluid/vapor at the high temperatures of Martian magmatism. However, the data from terrestrial systems (e.g., Edmonds 2015) obfuscates this hypothesis, and the partitioning of the LLEs in mineral-melt and fluid-melt systems has yet to be experimentally characterized for compositions and conditions relevant to the Martian mantle.

Existing experimental data suggest that Li and B and range from weakly to poorly volatile at conditions relevant to highly silicic magma chambers (Webster et al. 1989; Iveson et al. 2019). Experimental studies of Li and B partitioning in a hydrous basaltic system have not yet been conducted, as the majority of research in this area focuses on more evolved, shallow systems relevant to the formation of ore deposits. For instance, the rhyolitic melt experiments of Webster et al.1989 showed that Li is compatible in Cl-bearing aqueous fluids, reporting fluid-melt partition coefficients, i.e.,

$$D_{Li}^{fluid/melt} = \frac{Li\ in\ fluid}{Li\ in\ melt} \quad (2)$$

with values greater than one that increase as the Cl content of the fluid increases. Iveson (2019) also conducted fluid-melt Li partitioning experiments using dacitic to rhyolitic compositions at shallow crust conditions. Their conclusions disagree with Webster et al. 1989, finding that $D_{fluid/melt}$<1, with Li only becoming mobile in the fluid at very high Cl contents (>11 wt%) in highly silicic magma compositions that are not found on Mars. This raises the possibility that core-to-rim decreases in LLE concentrations in Martian cpx may record a process other than degassing. If, for instance, the compatibility of the LLEs changes as a function of temperature, cooling during crystal fractionation could induce reverse zoning patterns in cpx. Several authors have previously measured the partitioning of Li and B between basaltic minerals (here, cpx, orthopyroxene, plagioclase and garnet) and silicate melts in controlled experiments (see Table 1 for a compilation of cpx/melt partition coefficients). These studies have found B is strongly incompatible in crystalline phases (D<0.1) with Li behaving moderately incompatibly (0.1<D<1), with no systematic effect of temperature, pressure or bulk composition on measured partition coefficients. However, the published data have been collected from experiments performed over a limited range of pressures and temperature. In addition, there are no studies of LLE partitioning at high pressures (e.g., > 1 atm) in the Fe-rich compositions relevant to the Martian mantle.

Here we provide direct measurements of the partitioning of LLEs and other trace elements between melts and minerals in synthetic terrestrial and Martian basalts in experiments where temperature and pressure have been varied systematically. We use the experimental data to evaluate the hypothesis that LLE partition coefficients change as a function of temperature and/or pressure, such that "normal" igneous differentiation could produce the reverse zoning patterns observed in Martian and

Study	Phases	T (°C)	P (Gpa)	Li	1σ	B	1σ
Ottolini et al. (2009)	cpx	1330	1.0	0.246	0.018	0.041	0.020
Seitz (1973)	cpx	1150	2.0	-	-	0.071	0.036
Ryan (1989)	cpx	1150-1245	0.0001	0.145	0.350	0.090	0.080
Chaussidon and Libourel (1993)	cpx	1325-1450	1-1.5	-	-	0.117	0.012
Hart and Dunn (1993)	cpx	1380	3.0	0.590	0.070	0.036	0.020
Brenan et al. (1998)	cpx	1000-1350	1-1.5	0.270	0.100	0.025	0.006
Blundy et al. (1998)	cpx	1255	1.5	0.254	0.044	-	-
Schmidt et al. (1999)	cpx	1040	1.5	0.173	0.010	-	-
McDade et al. (2003)	cpx	1315	1.5	0.227	0.040	-	-
Herd et al. (2004)	cpx avg	1050-1300	0.0001	0.2	-	0.023	-

Table 1: Summary of reported partition coefficients for Li and B in cpx/melt

terrestrial rocks. While these measurements provide a broad basis to understand LLE behavior during crystallization, further experiments involving partitioning between minerals, melt and a fluid phase will be imperative to establish whether or not the LLEs are volatile at magmatic conditions on Mars.

METHODS

2.1 Experimental Methods

Partitioning experiments were conducted on synthetic terrestrial and Martian basalts. The synthetic terrestrial basalt, referred to as Mix 1 (Table 2), was mixed to approximate an average MORB composition based on experiments from Khitarov et al. 1968. The synthetic Martian basalt, Mix 2 (Table 2), was mixed to approximate the bulk composition of the meteorite NWA-480 (Barrat 2002). Reagents were added to each starting composition as oxides ($SiO_2, Mg_2SiO_4, TiO_2, Al_2O_3, Fe_2O_3, FeO, MnO$), carbonates ($CaCO_3, Na_2CO_3, K_2CO_3$) and phosphates ($CaPO_4$) and mixed under ethanol in an agate mortar and pestle. Each mix was then dried under a heat lamp, loaded into a platinum crucible and inserted into a kiln for decarbonation. During the decarbonation routine the kiln was ramped up to 800° C at 100° C/hour, held for 5 hours, ramped up to 1200° C at the same rate, held for one hour, and then removed from the kiln. The decarbonated powders were glassed in a 1 atm furnace at 1300° C in a platinum crucible. Mass loss after the glass step was negligible. The glasses were reground into a powder with the same mortar and pestle, then trace elements were added as either oxides (V, Sc, Cr, Y, Zr, Ru, Ge, Ga, Mo, Nb, Ta, Ni) or as ICP-MS solutions (Li, Be, B, Sr, Rb). About ~300 ppm of all trace elements were added to each composition, except Li which was doped at about ~500 ppm for easier detection with analytical instruments (Table 3). The mixes were denitrified in a drying oven at 110 °C and stored in a vacuum desiccator to mitigate any adsorption of water.

Composition	SiO_2	TiO_2	Al_2O_3	Fe_2O_3	FeO	MnO	MgO	CaO	Na_2O	K_2O	P_2O_5
Mix 1	52.1	0.82	15.2	4.48	5.16	0.1	9.49	9.29	2.46	0.89	0.13
Mix 2	51.1	1.09	5	0	21.6	0.51	9.92	8.35	1.26	0.3	0.53

Table 2: Bulk starting composition for terrestrial (Mix 1) and Martian (Mix 2) synthetic basalts

	V	Sc	Cr	Y	Zr	Ru	Ge	Ga	Mo	Nb	Ta	Ni	Rb	Be	B	Sr	Li
Conc. (ppm)	283	272	285	328	308	316	289	155	278	291	341	327	300	300	300	300	500

Table 3: Trace element starting concentrations for Mix 1 and 2

Experiment Conditions						
Experiment	Mix	Assembly	Capsule	T (°C)	P (Gpa)	t (hrs)*
bas1-8	1	$BaCO_3$	C	1175	1	46.2
bas1-5	1	$BaCO_3$	C	1225	1	80.5
bas1-10	1	$BaCO_3$	C	1275	1	40.8
bas1-13	1	$BaCO_3$	C	1225	0.8	55.5
bas1-6	1	$BaCO_3$	C	1225	1.5	54.5
bas2-6	2	$BaCO_3$	C	1175	1	21.2
bas2-1	2	$BaCO_3$	C	1225	1	103.5
bas2-8	2	$BaCO_3$	C	1225	0.8	57.5
bas2-2	2	$BaCO_3$	C	1225	1.5	53.5
bas2-7	2	$BaCO_3$	C	1225	1.5	28.5

*Table 4: Experiment conditions. *t=total run time - temperature cycle run time*

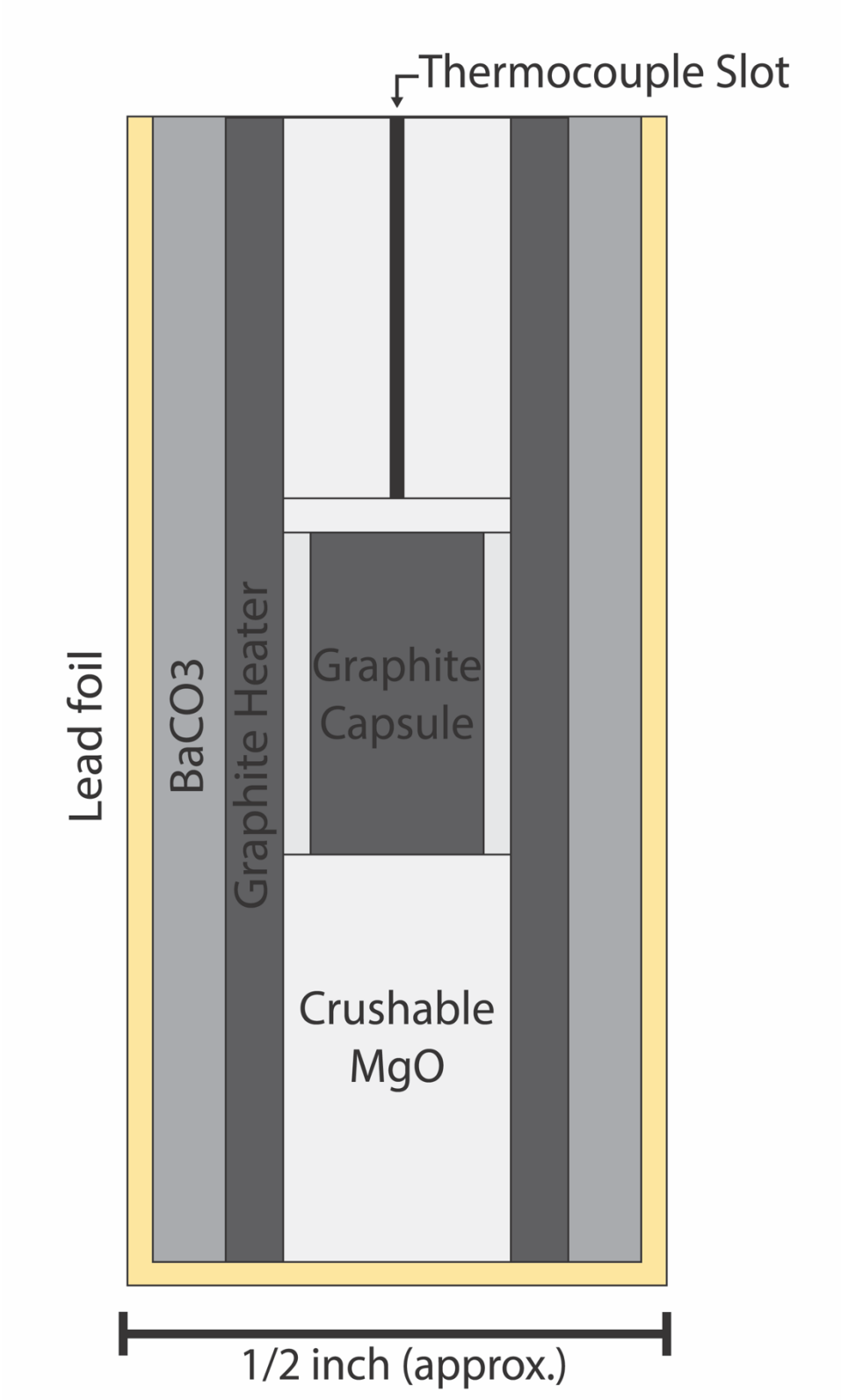

Figure 1: Barium Carbonate Assembly (Not to Scale)

Piston-cylinder experiments were run between 1125-1225° C and 0.8-1.5 GPa (see Table 4 for a complete list of run conditions). The desired mix was loaded into a machined graphite capsule and placed into an Al_2O_3 sleeve. Graphite heaters, MgO crushable pressure media and $BaCO_3$ hydrostatic pressure cells were used in all assemblies (Figure 1). The MgO was fired to remove any water before placement in the assembly. Lead foil was placed around the $BaCO_3$ pressure media in all experiments.

Piston-cylinder assemblies were cold pressurized to targeted run pressure before heating. A schematic of the piston-cylinder press is provided in Figure 2. Experiment temperatures were ramped at rate of 75° C/min to 1300° C where they dwelled for one hour. A temperature cycle was used to promote crystal growth; experiments were ramped down to the target temperature at 1° C/min. The temperature was then ramped +15° and -15° from the target temperature at 0.1° C/min, before finally being brought back to the target temperature at 0.1° C/min. Experiments were held at the target temperature for ~21-103 hours following each temperature cycle. Temperature cycling took between 9-26 hours, dependent on the target temperature. Experiment pressure was adjusted as needed once experiments reached the target temperature. Experiments were quenched isobarically by cutting power to the experiment and manually holding the pressure steady. Quenched experiments were pressed out of the piston-cylinder assembly, the capsule extracted and mounted in epoxy. They were then ground parallel to the long axis of the capsule to maximize the amount of exposed material and impregnated with epoxy in a pressure vessel. Once cured, the epoxy discs were polished using 240-1200 grit SiC paper followed by 5 and 1 μm alumina.

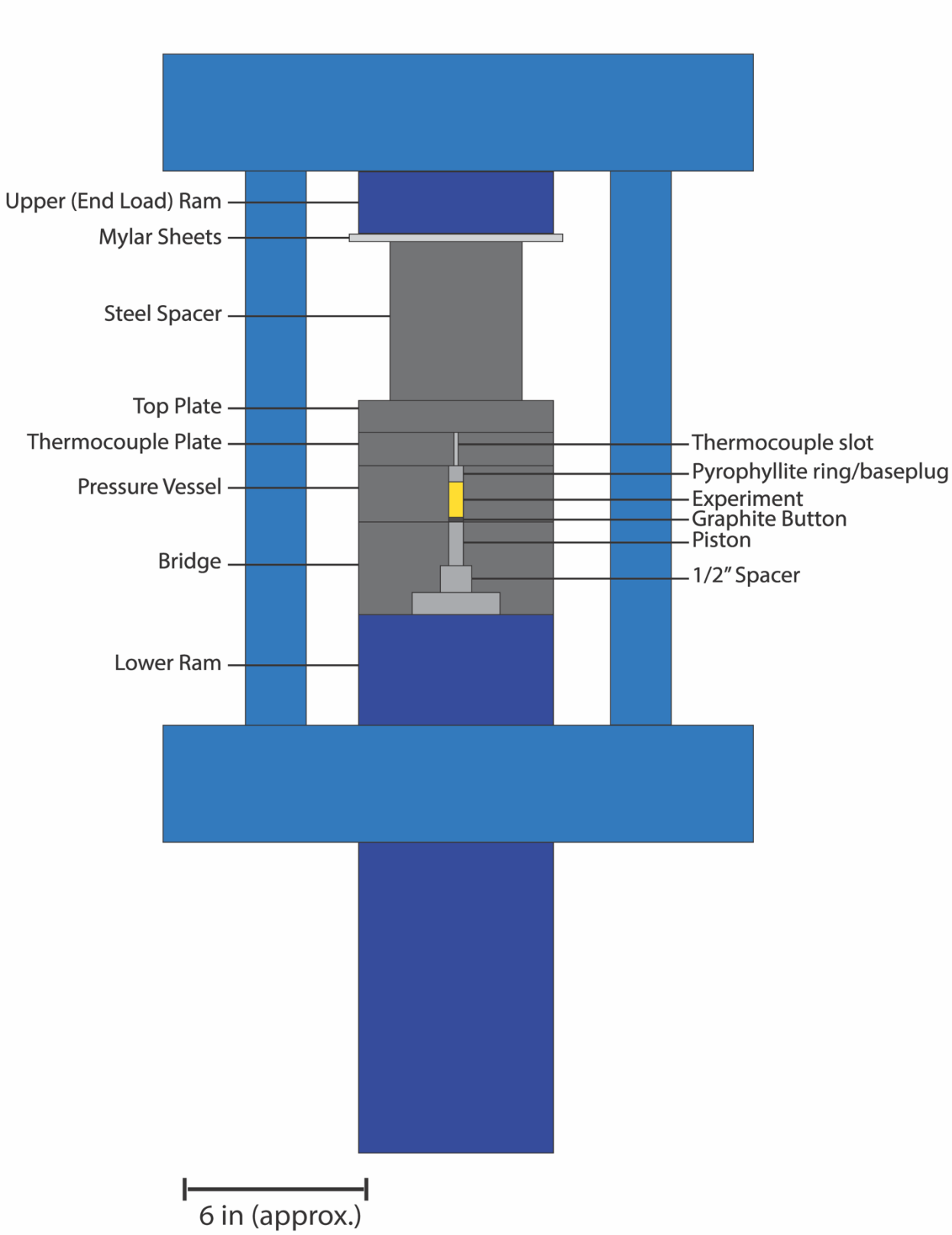

Figure 2: Schematic of the Piston Cylinder Apparatus (Not to scale)

2.2 Analytical Methods

The major element compositions of all experiments were measured using the Cameca SXFive Electron Probe at Syracuse University. Si, Ti, Al, Fe, Mn, Mg, Ca, Na, K and P in experimental minerals and glasses were measured using an accelerating voltage of 15 kV and a beam current of 10 nA. Minerals were analyzed using a focused (0 μm) spot size and glasses were analyzed with a 10 μm spot size. Smithsonian glass standards A-99 and VG-2 were used as secondary standards to confirm the accuracy of glass analyses. Augite, plagioclase (Smithsonian Institution) and enstatite (Astimex) were used as secondary standards to confirm the accuracy of mineral analyses.

Trace elements (V, Sc, Cr, Y, Zr, Ru, Ge, Ga, Mo, Nb, Ta, Ni, Rb, Sr, B, Be, Li) were measured in the experimental minerals and glasses using LA-ICP-MS. We performed laser analyses in two laboratories. A subset of experiments were analyzed with the Photon Machines 193 nm laser and Agilent 7900 ICP-MS at the University of Rochester. A second set of experiments were analyzed with the Agilent 8900 ICP-MS/MS and ESI NWR 193HE laser at Cornell University. Laser data were collected in single quadrupole mode. Experimental glasses at Rochester were ablated at a fluence of 5.73 J/cm^2 and a 10 Hz rep rate using a 40 μm circular spot. Minerals were ablated at a fluence of 6.75 and a 7 Hz rep rate with a 15 μm or 10 μm circular spot size. NIST610, 612 and 614 glasses were used as the standard for glass analyses with omphacite (Smithsonian Institution) used as a secondary standard for crystal analyses. LA-ICP-MS data were reduced in the Iolite 4 software package using ^{29}Si as the internal standard in the 3D trace element data reduction scheme. Samples were ablated

for 30 s, followed by 20 s of background collection. Standards bracketed ablation of unknowns and were run about every five samples. He was used as the carrier gas for the laser aerosol.

All mineral ICP-MS spectra were carefully examined for signs of contamination by silicate melt. The small size of the crystals in several of the experiments limited LA-ICP-MS analyses to n=1 or 2 analyses from each phase.

RESULTS

3.1 Phase Assemblages

The synthetic terrestrial basalt, Mix 1, produced phase assemblages consisting of garnet, clinopyroxene, orthopyroxene, and plagioclase. At 1175 °C and 1 GPa, opx and cpx were present; opx alone crystallized at 1225 °C and 0.8 GPa; opx, cpx, and plag were present at 1225° and 1275° C and 1 GPa; garnet, cpx, and plag were present at 1225° C and 1.5 GPa. Phase assemblages for Mix 1 are depicted in temperature and pressure space in Figure 3. Clinopyroxene was the sole phase present in all experiments run using Mix 2. The major and minor element compositions of all experimental phases are presented in Table 5. Backscattered electron images of representative samples are shown in Figure 4.

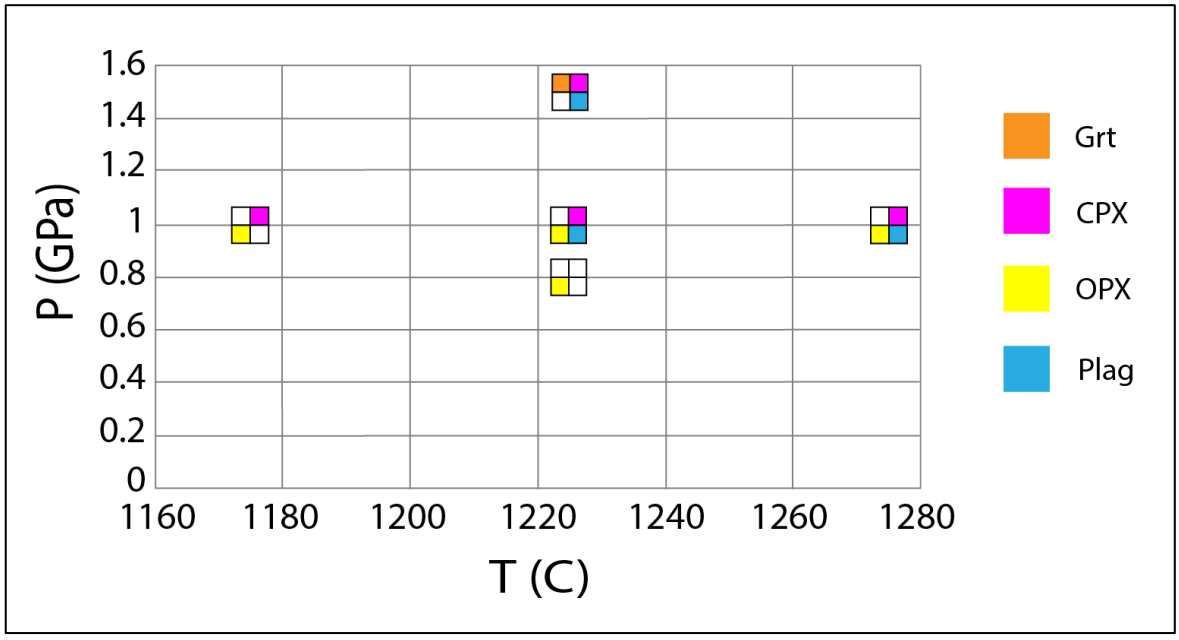

Figure 3: Phases in P and T space for Mix 1 (terrestrial)

expt; phase	T (°C)	P (GPa)	n	SiO2	SD	TiO2	SD	Al2O3	SD	FeO	SD	MnO	SD	MgO	SD	CaO	SD	Na2O	SD	K2O	SD	P2O5	SD	Total
bas1-5 glass	1225	1	68	49.76	1.08	1.04	0.07	17.22	0.41	9.88	0.53	0.09	0.02	5.96	0.24	9.10	0.25	3.17	0.28	0.39	0.04	0.19	0.04	96.79
bas1-6 glass	1225	1.5	43	55.04	0.56	1.15	0.06	17.60	0.38	7.60	0.15	0.04	0.01	4.03	0.24	6.93	0.16	4.42	0.26	0.65	0.04	0.17	0.03	97.62
bas1-8 glass	1275	1	19	51.01	0.96	1.22	0.29	18.42	2.78	9.81	2.23	0.07	0.02	4.53	0.99	8.32	0.88	3.86	0.32	0.60	0.11	0.16	0.04	97.91
bas1-10 glass	1175	1	39	49.30	0.36	0.91	0.03	17.24	0.48	9.22	0.15	0.07	0.02	8.12	0.11	9.83	0.07	3.33	0.21	0.37	0.01	0.13	0.01	98.52
bas1-13 glass	1225	0.8	22	50.78	0.53	0.88	0.03	16.33	0.30	9.36	0.22	0.10	0.02	7.74	0.21	9.56	0.14	2.67	0.18	0.35	0.02	0.14	0.02	97.92
bas2-1 glass	1225	1	40	48.72	0.83	1.66	0.07	7.57	0.37	20.48	0.83	0.32	0.02	5.89	0.27	9.03	0.23	2.21	0.20	0.39	0.04	0.64	0.04	96.92
bas2-2 glass	1275	1	45	42.50	0.28	1.92	0.03	7.85	0.27	27.08	0.26	0.31	0.02	4.46	0.07	8.28	0.06	2.22	0.14	0.45	0.02	0.76	0.04	95.81
bas2-6 glass	1175	1	6	46.54	0.24	1.83	0.04	8.15	0.17	22.71	0.22	0.39	0.04	4.19	0.05	8.04	0.07	2.26	0.06	0.52	0.02	0.89	0.05	95.53
bas2-7 glass	1225	1.5	6	43.20	0.22	2.03	0.06	7.76	0.24	25.67	0.15	0.40	0.02	4.12	0.07	7.92	0.07	2.11	0.14	0.52	0.02	1.07	0.07	94.79
bas2-8 glass	1225	0.8	25	47.17	0.52	1.42	0.04	6.36	0.27	23.30	0.28	0.45	0.03	6.47	0.13	9.24	0.09	1.61	0.15	0.33	0.03	0.70	0.04	97.05
bas1-5 plag	1225	1	8	51.80	0.34	0.03	0.01	30.64	0.44	0.35	0.13	0.00	0.01	0.30	0.37	13.81	0.16	3.71	0.22	0.09	0.01	0.01	0.01	100.76
bas1-8 plag	1275	1	6	53.83	0.62	0.06	0.04	28.71	1.25	0.99	0.98	0.02	0.02	0.80	1.31	11.78	0.68	4.50	0.44	0.15	0.02	0.01	0.01	100.86
bas1-5 cpx	1225	1	5	50.18	0.91	0.52	0.08	7.74	1.38	7.87	0.11	0.11	0.02	16.44	0.48	16.94	0.22	0.56	0.06	0.00	0.00	0.02	0.02	100.39
bas1-6 CPX	1225	1.5	6	49.73	1.35	0.68	0.37	11.63	1.33	10.31	0.41	0.10	0.02	13.59	2.16	13.48	1.28	1.32	0.57	0.04	0.09	0.06	0.10	100.94
bas1-8 cpx	1275	1	7	51.35	0.46	0.37	0.03	6.98	0.73	13.20	1.17	0.14	0.02	22.66	0.91	5.21	0.39	0.20	0.06	0.01	0.01	0.02	0.01	100.14
bas1-10 cpx	1175	1	6	50.38	0.57	0.36	0.06	8.51	0.85	7.74	0.68	0.11	0.02	17.82	0.92	14.51	1.32	0.63	0.08	0.00	0.00	0.01	0.01	100.08
bas1-5 opx	1225	1	53	53.07	0.73	0.19	0.03	5.82	0.63	11.18	0.84	0.11	0.01	28.21	0.82	2.10	0.13	0.08	0.03	0.00	0.00	0.00	0.01	100.75
bas1-10 opx	1175	1	3	52.87	0.79	0.16	0.01	6.55	0.97	10.46	0.38	0.10	0.01	28.05	0.63	2.18	0.07	0.13	0.02	0.00	0.01	0.01	0.01	100.51
bas1-13 opx	1225	0.8	33	54.08	0.72	0.17	0.03	5.33	0.94	10.69	0.55	0.12	0.02	28.10	0.84	2.12	0.21	0.07	0.03	0.01	0.00	0.00	0.01	100.70
bas1-6 garnet	1225	1.5	23	40.40	0.29	0.62	0.13	22.82	0.24	16.89	0.69	0.22	0.02	14.19	0.41	6.09	0.14	0.04	0.04	0.00	0.01	0.05	0.01	101.33
bas2-1 cpx	1225	1	6	52.81	0.27	0.17	0.03	0.83	0.22	20.14	0.42	0.55	0.02	18.66	0.68	7.28	1.03	0.11	0.07	0.00	0.01	0.02	0.02	100.58
bas2-2 cpx	1275	1	66	52.00	0.42	0.18	0.03	1.31	0.22	22.17	0.46	0.51	0.02	16.93	0.78	7.13	0.65	0.26	0.05	0.00	0.01	0.01	0.01	100.50
bas2-6 cpx	1175	1	6	51.36	0.70	0.21	0.04	1.07	0.21	23.89	0.92	0.56	0.02	15.63	0.82	6.93	1.01	0.16	0.06	0.00	0.00	0.01	0.01	99.82
bas2-7 cpx	1225	1.5	7	50.96	0.54	0.18	0.04	1.57	0.30	24.58	0.85	0.51	0.02	14.67	0.85	6.78	0.32	0.38	0.06	0.00	0.00	0.00	0.01	99.65
bas2-8 cpx	1225	0.8	45	53.69	0.44	0.13	0.02	0.58	0.09	20.85	0.83	0.53	0.04	20.69	1.45	4.27	0.94	0.10	0.04	0.00	0.01	0.00	0.01	100.85

Table 5: Major and minor element compositions of all experimental phases. SD = Standard Deviation

Clinopyroxene compositions ranged from 32.4-36.9% Wo, 43.8-58.4% En, and 13.2-19.6% Fs in Mix 1 and 8.7-15.8% Wo, 46.4-49.8% En, and 32.1-41.4% Fs in Mix 2 (see Table 6). Mix 1 cpx are augitic while Mix 2 cpx are primarily pigeonite.

	Wo%	En%	Fs%	Total
bas2-1	14.9	53.0	32.1	100.0
bas2-2	15.8	43.8	40.5	100.0
bas2-6	14.6	46.0	39.4	100.0
bas2-7	14.6	44.0	41.4	100.0
bas2-8	8.7	58.4	33.0	100.0
bas1-5	36.9	49.8	13.4	100.0
bas1-6	33.3	46.8	19.9	100.0
bas1-8	34.1	46.3	19.6	100.0
bas1-10	32.4	54.4	13.2	100.0

Table 6: Cpx compositions for all experiments

3.2 Partition Coefficients

All trace element partition coefficients were determined by LA-ICP-MS measurements from ~10 glass spots and ~1-10 crystal analyses for each phase present in the experiments. Mineral-melt partition coefficients were calculated using values from LA-ICP-MS measurements using equation 1. Partition coefficient standard errors were calculated using the mean and standard deviation of LA-ICP-MS measurements (for n>2) with the following equation:

$$SE = D^{min/melt} \times \sqrt{\left(\left(\frac{SD\ melt}{mean\ melt}\right)^2 + \left(\frac{SD\ min}{mean\ min}\right)^2\right)} \qquad (3)$$

All calculated partition coefficients are reported in Table 7.

Sample	Phase	T	P	Li	SE	Be	SE	B	SE	P	SE	Sc	SE	V	SE	Cr	SE	Ni	SE	Ga	SE
bas2-2	cpx	1225	1.5	0.667	0.049																
bas2-6	cpx	1175	1	0.236	0.006	0.015	0.002	0.024	0.003	64.908	1.359	0.065	1.177	1.198	0.032	5103.235	133.051	0.195	0.006	0.520	0.015
bas2-1	cpx	1225	1	0.543	0.053																
bas2-7	cpx	1225	1.5	0.758	0.102																
bas2-8	cpx	1225	0.8	0.440	0.027																
bas1-5	plag	1225	1	0.192	0.006	0.142	0.010	0.047	0.003			0.036	437.879	0.021	0.002	2496.905	131.313	0.004	0.001	0.009	0.004
bas1-8	plag	1175	1	0.607		0.286		0.054		0.142		0.536		1.506		5.755		0.880		1.888	
bas1-10	cpx	1275	1	0.335	0.019	0.029	0.002	0.025	0.006			0.009	432.025	2.071	0.182	6852.190	515.982	0.929	0.082	1.274	0.143
bas1-8	cpx	1175	1	0.600		0.247		0.074		0.120		1.973		3.668		8.706		2.762		1.789	
bas1-5	cpx	1225	1	0.284		0.036		0.045		0.043		2.664		5.424		21.517		1.529		0.626	
bas1-6	cpx	1225	1.5	0.918		0.123		0.123		610.781		0.922		4.243		21322.543		2.363		2.740	
avg				0.534	0.019	0.109	0.002	0.067	0.006												
					0.291				0.043												
bas1-6	gar	1225	1.5	0.113	0.043	0.004	0.004	0.013	0.009	496.291	54.631	0.707	610.691	10.251	2.024	45237.437	7261.886	1.311	0.288	1.661	0.351
bas1-5	opx	1225	1	0.202	0.014	0.020	0.004	0.050	0.009	395.669	44.945	0.047	73.565	1.848	0.189	5300.748	691.458	0.881	0.127	2.372	0.226
bas1-13	opx	1225	0.8	0.425	0.034	0.037	0.004	0.037	0.008	0.077	0.032	2.997	0.311	7.521	0.583	27.084	3.554	6.754	0.654	1.008	0.127
bas1-10	opx (2)	1275	1	0.255	0.019	0.025	0.009	0.023	0.021	0.038	0.001	1.089	2762.991	2.419	0.220	9.608	1.222	1.939	0.154	0.534	0.128

Sample	Phase	T	P	Ge	SE	Rb	SE	Sr	SE	Y	SE	Zr	SE	Nb	SE	Mo	SE	Ta	SE
bas2-2	cpx	1225	1.5																
bas2-6	cpx	1175	1	8.549	0.156	0.217	0.008	0.453	0.022	0.002	0.003	0.010	0.001	0.125	0.006	0.035	0.003	0.002	0.002
bas2-1	cpx	1225	1																
bas2-7	cpx	1225	1.5																
bas2-8	cpx	1225	0.8																
bas1-5	plag	1225	1	0.054	0.008	1.649	0.100	0.458	0.031	0.026	0.003	0.686	0.078	0.009	0.001	0.001	0.001	0.000	0.0004
bas1-8	plag	1175	1	1.696		0.065		2.990		0.095		0.027		0.013		0.026		0.017	
bas1-10	cpx	1275	1	3.552	0.645	1.326	0.067	1.240	0.066	0.000	0.001	0.010	0.001	0.709	0.082	0.681	0.104	0.007	0.002
bas1-8	cpx	1175	1	2.456		0.042		1.813		0.409		0.124		0.021		0.045		0.032	
bas1-5	cpx	1225	1	1.647		0.002		0.057		0.840		0.194		0.010		0.039		0.027	
bas1-6	cpx	1225	1.5	12.369		1.530		1.512		0.156		0.038		0.189		0.230		0.077	
avg																			
bas1-6	gar	1225	1.5	8.939	0.899	1.496	0.136	2.336	0.237	0.004	0.011	0.001	0.002	3.988	0.651	1.937	0.283	0.010	0.006
bas1-5	opx	1225	1	7.005	0.530	0.790	0.083	1.299	0.103	0.005	0.006	0.005	0.005	0.110	0.019	0.056	0.014	0.005	0.005
bas1-13	opx	1225	0.8	2.927	0.212	0.001	0.003	0.003	0.001	0.260	0.030	0.069	0.010	0.003	0.002	0.043	0.006	0.006	0.002
bas1-10	opx (2)	1275	1	1.310	0.253	0.014	0.001	0.009	0.001	0.111	0.086	0.027	0.019	0.010	0.002	0.026	0.011	0.010	0.007

Table 7: Partition coefficients of trace elements for all available phases in each experiment. SE = Standard Error.

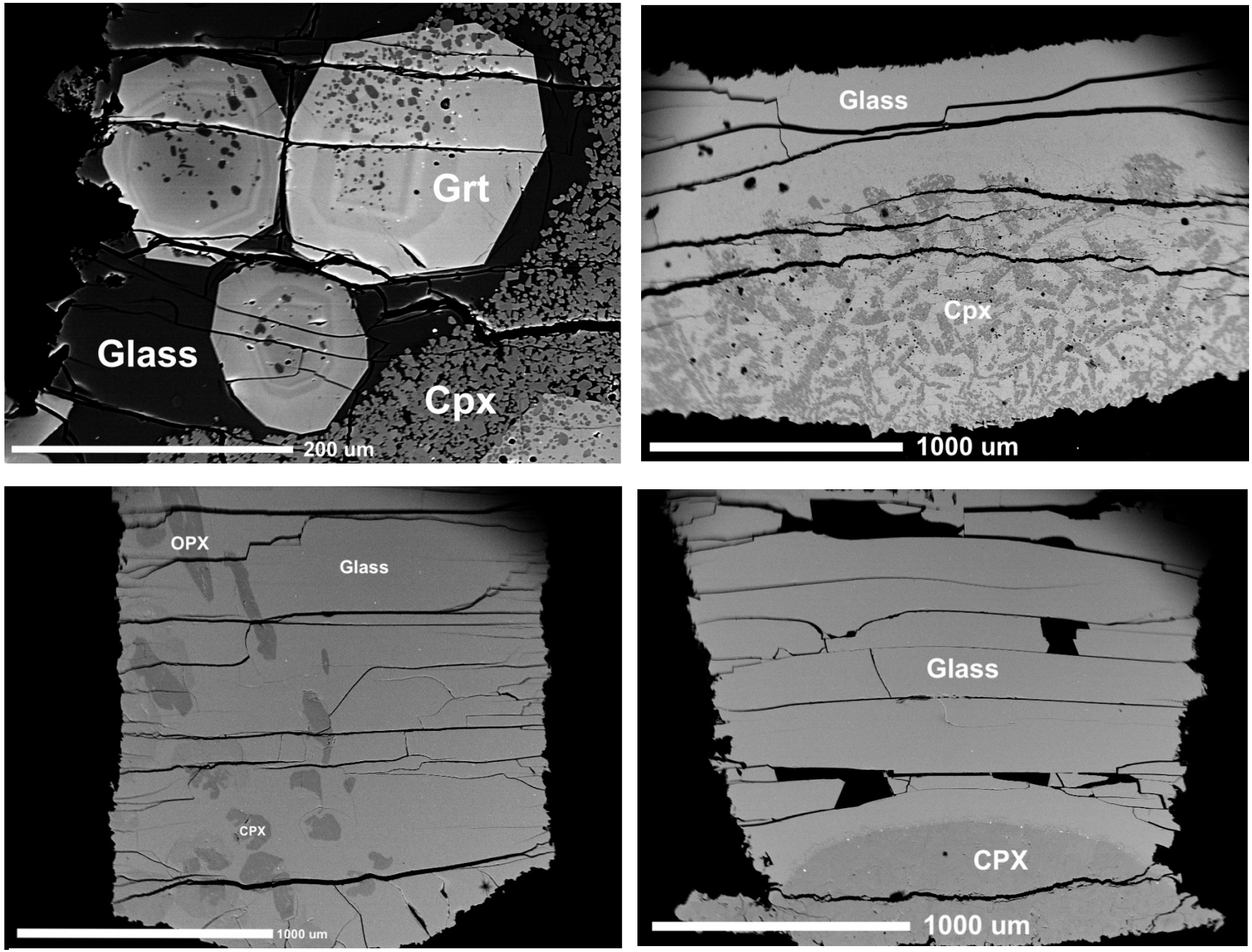

Figure 4: BSE images of selected experiments, bas1-6 (top left), bas1-8 (top right), bas1-10 (bottom left), bas2-1 (bottom right)

DISCUSSION

Although we have calculated partition coefficients for many trace elements in different mineral phases, here we focus the discussion on the behavior of Li in cpx to address the hypothesis that the reverse zoning in Martian cpx may be due to the changing compatibility of Li during cooling and/or decompression.

4.1 Lithium Partitioning in Cpx

We compare our new average $D_{Li}^{cpx/melt}$ values for each composition with previous average values from the literature in Figure 5. Our new $D_{Li}^{cpx/melt}$ values

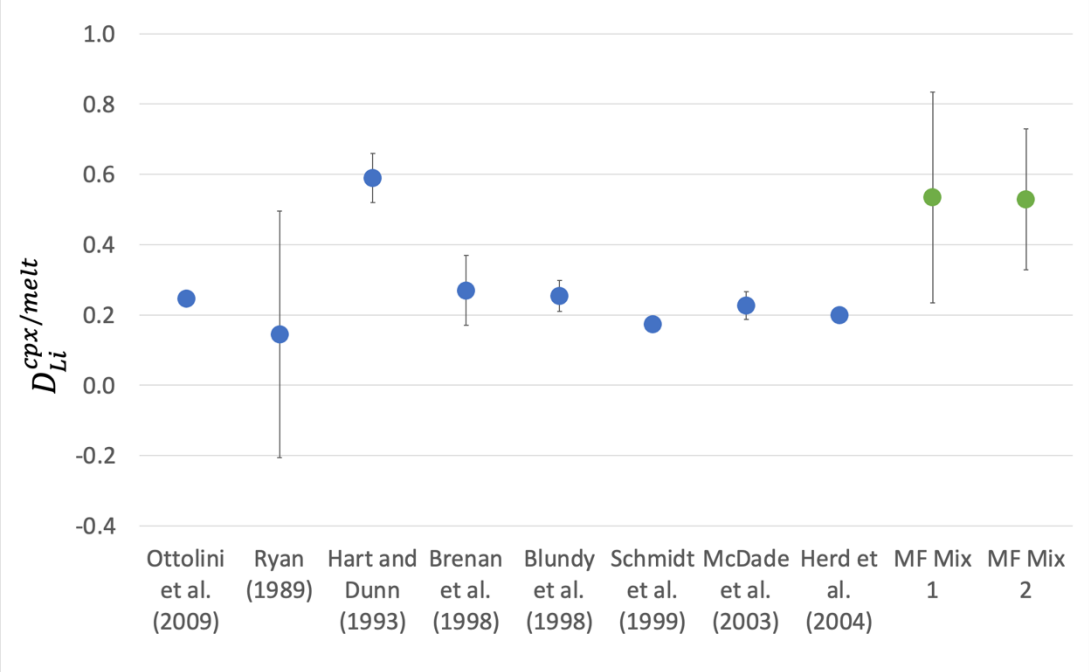

Figure 5: Average $D_{Li}^{cpx/melt}$ values from literature compared to new values from this study (green). Error bars represent the standard deviation from all experiments in each study.

extended to higher values compared to all previous studies except Hart and Dunn

(1993). The offset between our new values and the literature data is discussed in detail below.

4.1.1 Possible trends with temperature

Here we examine partition coefficients calculated for experiments run at constant pressure (1 GPa) to investigate the possibility that Li compatibility in cpx changes as a function of temperature. Both compositions show apparent trends with temperature, where $D_{Li}^{cpx/melt}$ for Mix 1 decreases with temperature and Mix 2 increases (Figure 6). Assuming that these trends are real, and not the result of

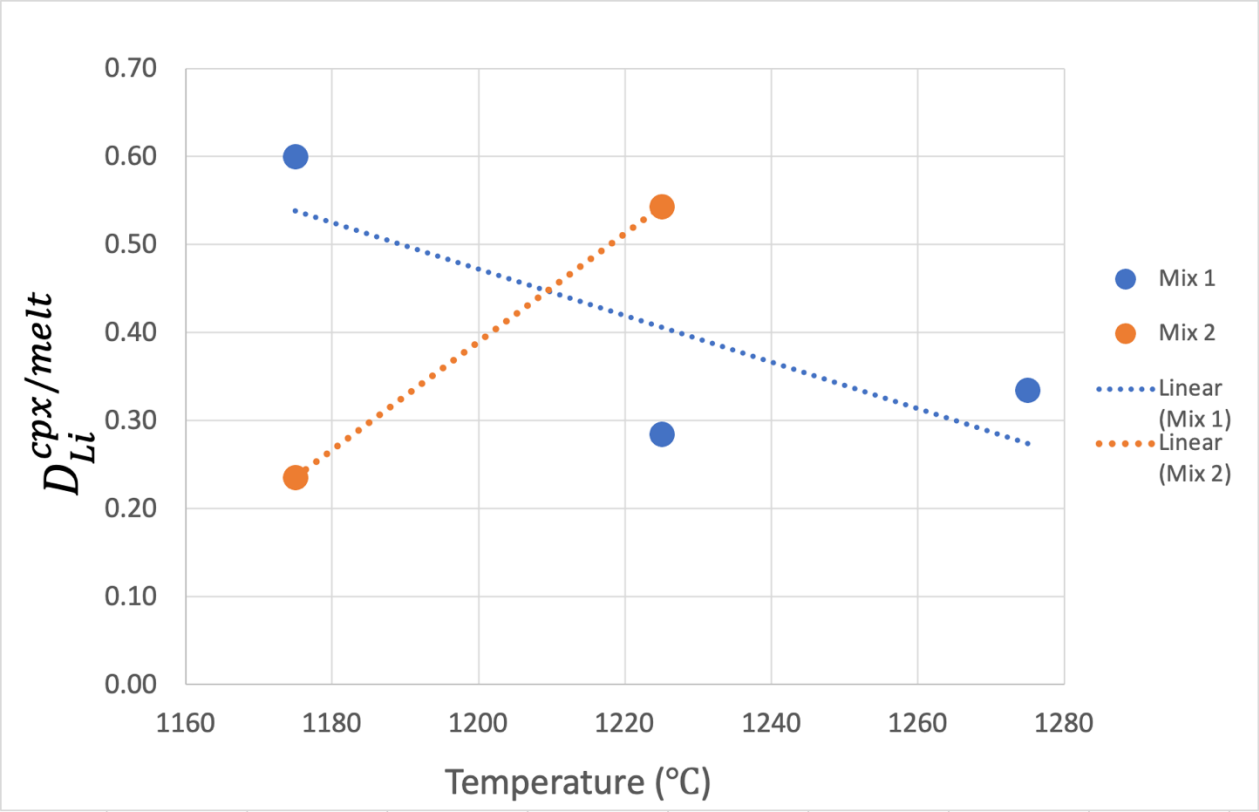

Figure 6: $D_{Li}^{cpx/melt}$ plotted against temperature in °C at 1 GPa.

erroneous LA-ICP-MS analyses, we find no thermodynamic explanation why Li

would become more compatible in cpx with decreasing temperature in the terrestrial basaltic bulk composition and less compatible in cpx with decreasing temperature in the Martian basaltic bulk composition. We suggest that the high $D_{Li}^{cpx/melt}$ for the Mix 1 experiment conducted at 1175 °C may be revised to a lower value with additional LA-ICP-MS analyses, as this partition coefficient was calculated using n=1 analyses of the cpx. Future work will focus on extending the temperature range of both the Mix 1 and Mix 2 experiments at 1 GPa.

Our data at 1 GPa is compared to the literature trend in Figure 7. Here we plot average $D_{Li}^{cpx/melt}$ values against average experiment temperature for studies reported in Table 1. We note that the literature experiments plotted in Fig. 7 have been conducted at pressures other than 1 GPa using a variety of bulk compositions, so we cannot rule out the additional effect of changing pressure or cpx composition on partition coefficient trends. Overall, there is a weak trend that suggests the compatibility of Li in cpx may decrease as experiment temperature decreases.

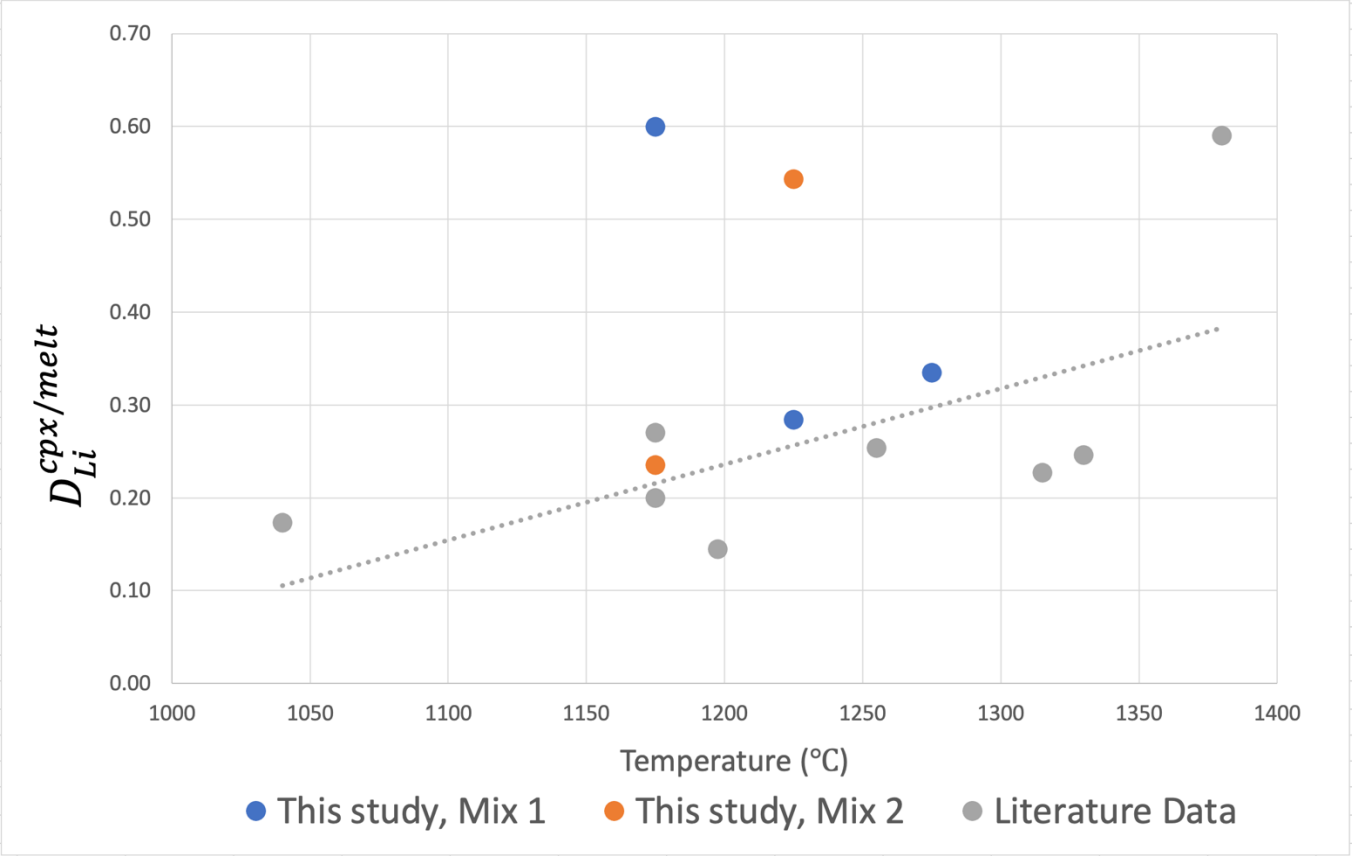

Figure 7: $D_{Li}^{cpx/melt}$ for literature data and this study plotted against temperature (℃)

4.1.2 Possible trends with pressure

Here we examine partition coefficients calculated for experiments run at constant temperature (1225 °C) to investigate the possibility that Li compatibility in cpx changes as a function of pressure. We observe $D_{Li}^{cpx/melt}$ increases as pressure increases for both compositions (Figure 8). This trend has not been previously recognized by other studies.

Our partition coefficients from experiments conducted at 1225 °C are compared to literature data as a function of pressure in Figure 9. Here we plot average $D_{Li}^{cpx/melt}$ values against average experiment pressure for studies reported in Table 1.

We note that the literature experiments plotted in Fig. 9 have been conducted at temperatures other than 1225 °C using a variety of bulk compositions, so we cannot rule out the additional effect of changing temperature or cpx composition on partition coefficient trends. Overall, there is a reasonably strong correlation (R^2=0.64) between $D_{Li}^{cpx/melt}$ and pressure for the literature data even though we cannot isolate the effect of changing pressure from changing temperature in this data set. The trend in the literature data reflect those of our experiments, where $D_{Li}^{cpx/melt}$ increases as pressure increases.

Lithium is predicted to substitute for Na on the clinopyroxene M2 site (e.g., Brenan et al. 1998). The ionic radius of Li (0.92 angstroms; Shannon 1976) is smaller than the ideal radius of the clinopyroxene M2 site (1.05 angstroms). Thus, increasing pressure should decrease the ideal radius of the M2 site, making it more energetically favorable for Li to be incorporated in cpx.

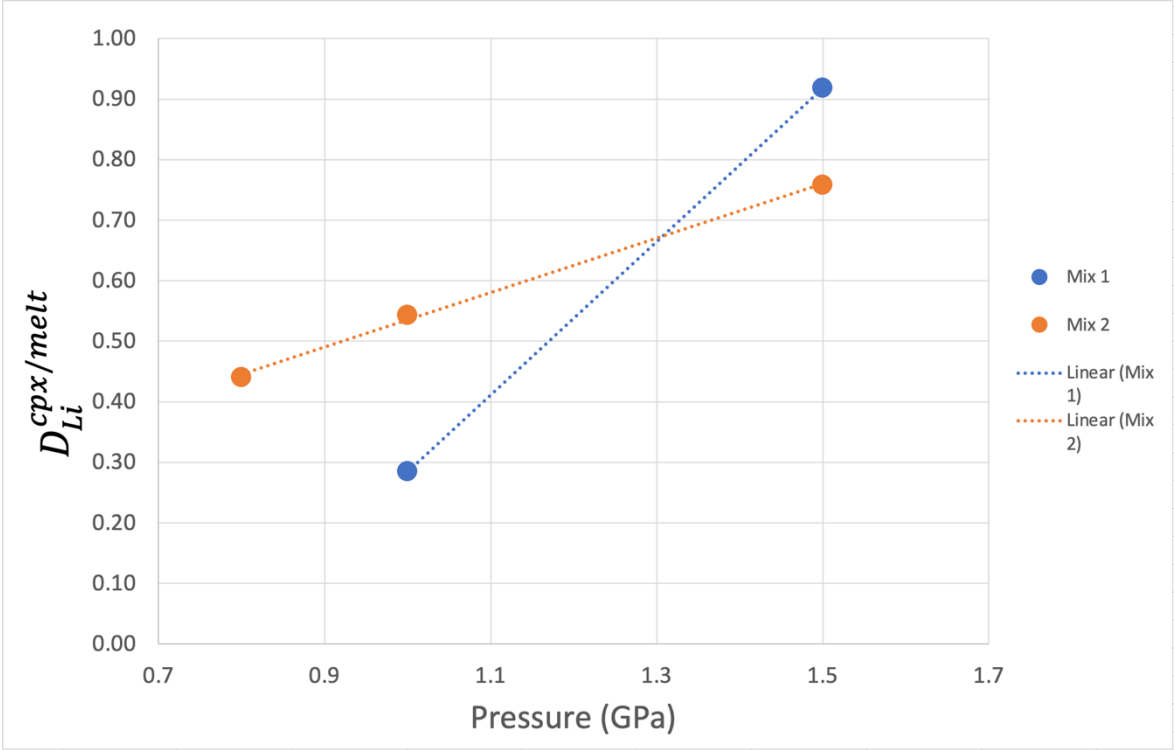

Figure 8: $D_{Li}^{cpx/melt}$ plotted against pressure in GPa at 1225 ℃

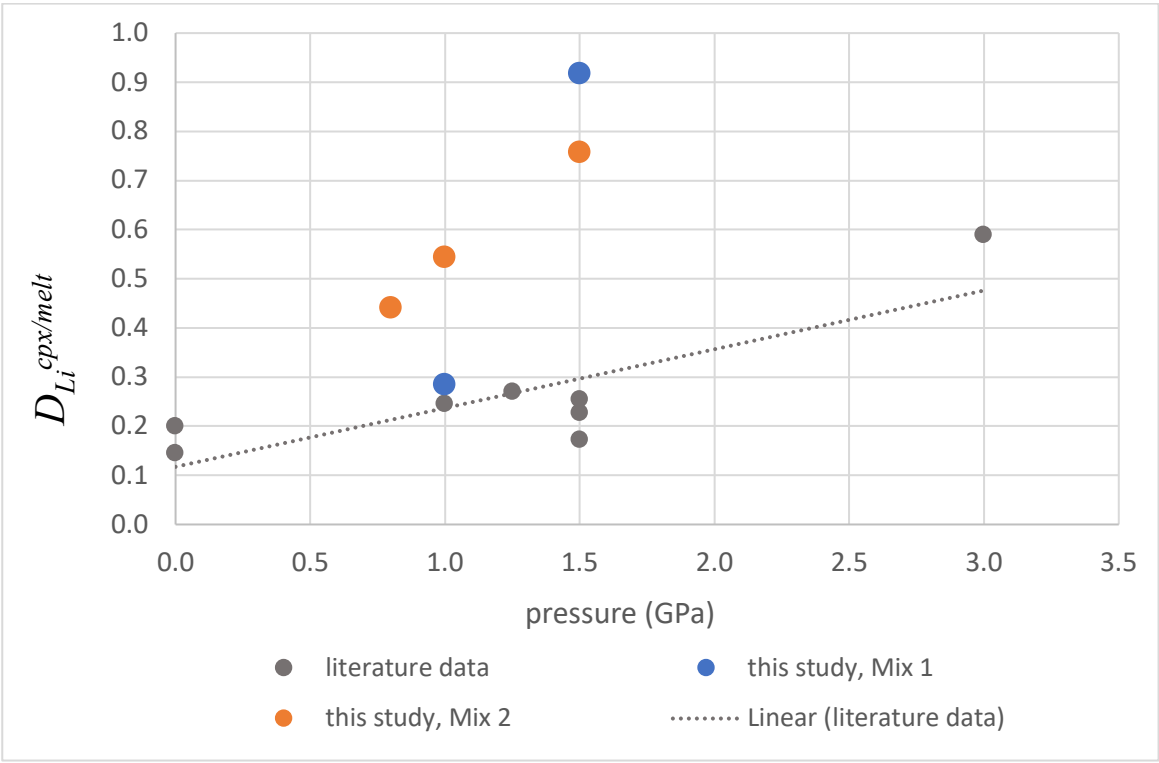

Figure 9: Literature data and this study, $D_{Li}^{cpx/melt}$ plotted against pressure in GPa at 1225 ℃

4.1.3 Possible trends with cpx composition

We observe an increase in $D_{Li}^{cpx/melt}$ as pressure increases at constant temperature in both experimental compositions. However, it is not clear if this correlation is truly a result of a pressure dependence on Li partitioning in cpx, or if this trend can be attributed to changing cpx solid solution as pressure increases (Table 6). Brenan et al. (1998) posed the idea that Li substitutes for Na because the charge and ionic radii of both elements are similar. This idea was supported by an excellent correlation between $D_{Li}^{cpx/melt}$ to $D_{Na}^{cpx/melt}$ in three experiments of Brenan et al. (1998). We plotted $D_{Li}^{cpx/melt}$ against $D_{Na}^{cpx/melt}$ to see if the trend of Brenan et al. (1998) is reflected in our data set (Figure 10). On average, $D_{Li}^{cpx/melt}$ increases with

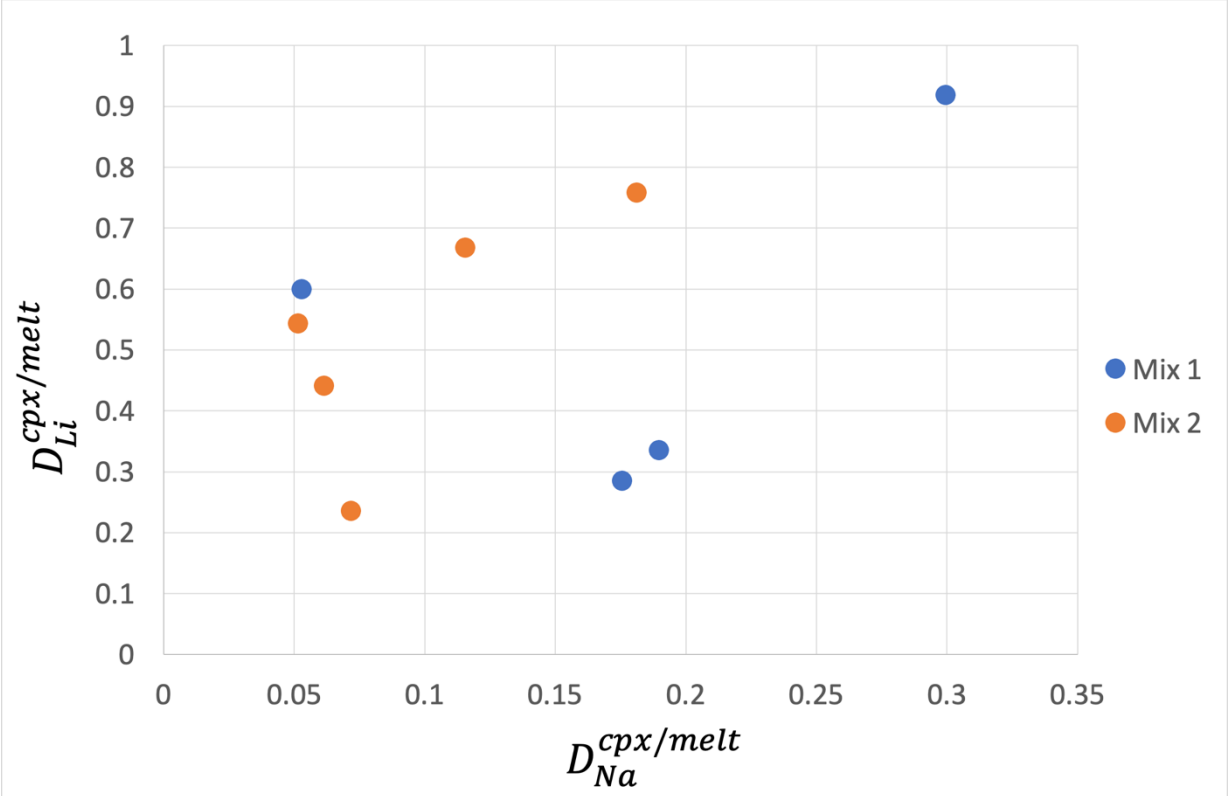

Figure 10: $D_{Na}^{cpx/melt}$ versus $D_{Li}^{cpx/melt}$ for mix 1 and mix 2.

increasing $D_{Na}^{cpx/melt}$, but the correlation is poor. The weak correlation may be in part the result of Li migration in the quenched glass under the electron beam during probe analysis. This will result in lower than "true" analyzed values of Na_2O in the glass and erroneous calculated partition coefficients. We do, however, find an excellent correlation between pressure and cpx Na_2O content across our pressure series experiments (Figure 11) that matches the positive correlation for between $D_{Li}^{cpx/melt}$ and pressure. This is an expected trend, as it has been demonstrated many times in the literature that cpx jadeite component increases as a function of pressure (e.g., Blundy et al. 1995). We do not observe any other systematic trends between cpx components, pressure, and/or $D_{Li}^{cpx/melt}$ in our experiments.

The relationship between Na and Li and pressure suggests Li becomes more compatible in the Na-rich cpx solid solutions that are stabilized at high pressures.

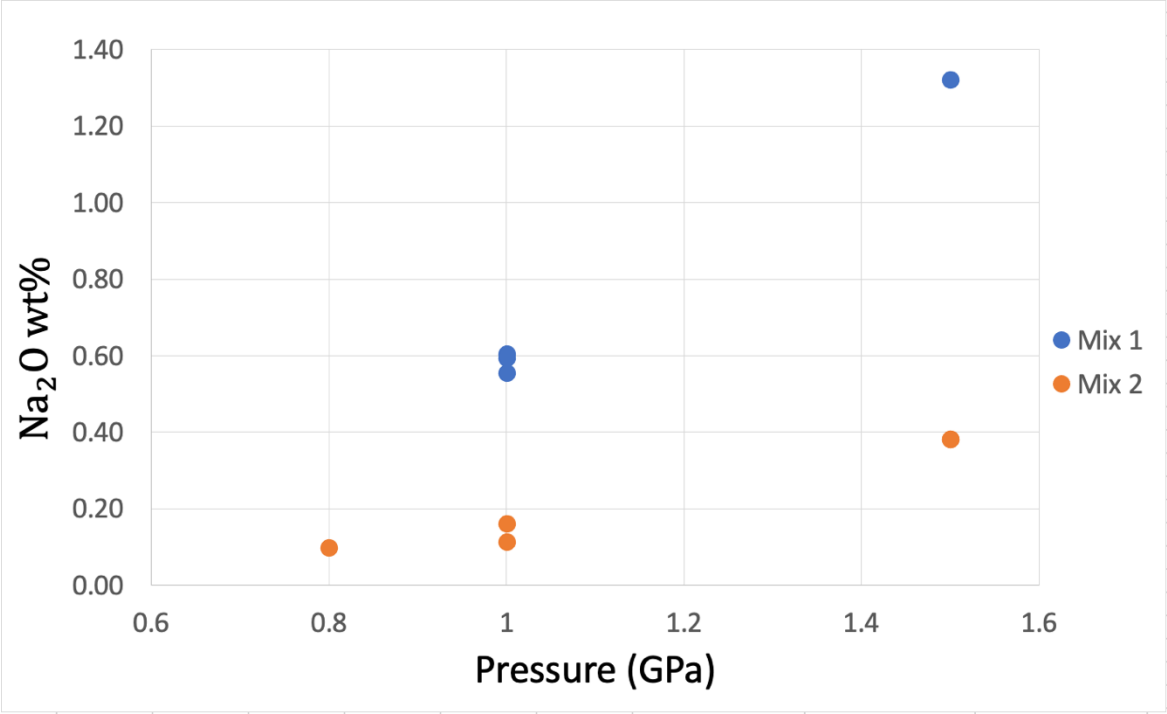

Figure 11: Weight percent Na_2O versus Pressure (GPa) for Mix 1 and Mix 2

However, the cpx crystallized from Mix 1 contain significantly more Na_2O compared to the cpx crystallized from Mix 2 (Figure 11), but the average compatibility of Li in cpx in each system is similar (Figure 5). This suggests that $D_{Na}^{cpx/melt}$ is more dominantly controlled by variations pressure and rather than cpx composition.

4.1.4 Possible trends with bulk composition

The average value of D_{Li} for all experiments is similar for both the Martian and terrestrial mix, about 0.5 for cpx (Figure 5). We conclude that bulk composition does not influence Li compatibility in cpx.

4.1.5 Comparison to previous studies

The Li partition coefficients we measure are more compatible on average than values previously reported in the literature, with the exception of Hart and Dunn (1993), see Tables 1 and 7 and Figure 5. Previous studies show $D_{Li}^{cpx/melt}$ to be around 0.2, independent of pressure and temperature, whereas our study and that of Hart and Dunn (1993) find $D_{Li}^{cpx/melt}$ to be closer to 0.5 (average across different P and T conditions). Our data also suggest $D_{Li}^{cpx/melt}$ is strongly pressure dependent and perhaps dependent on temperature as well. There are a few potential reasons for the offset between our results and the results of previous studies.

First, the experiments in this study were run at different pressure and temperature conditions that were varied systematically. Experiments run at 1 atm, such as Herd et al. (2004), reported that they experienced some Li loss to the atmosphere.

This suggests their experiments were not closed systems and may have been in disequilibrium. Brenan et al. (1998) ran experiments at a variety of temperatures (1000-1350 °C) and 1-1.5 GPa, but did not vary pressure or temperature systematically. This study would not be able to observe the same trends we see in our experiments without further experiments. Hart and Dunn (1993) ran Li partitioning experiments at 1380 °C and 3.0 GPa and reported a D_{Li} of 0.59, the closest value in the literature to our experiments. If the trend we see with pressure (and possibly temperature) in our experiments is real, this may explain why their experiments yielded high values of $D_{Li}^{cpx/melt}$ at higher pressures.

Our experiments were also held at target temperatures for longer periods of time than other studies (between ~21-104 hours; see Table 4). For example, Brenan et al. (1998) held their experiments at their "soaking" temperature for 3-24 hours; Herd et al. 2004 ran sets of experiments with run times between 1-24 hours, except one experiment which ran for 48 hours. It is possible that experiments in previous studies did not reach kinetic equilibrium between minerals and melts during their shorter runs, although this may be unlikely considering the fast diffusivities measured for Li in silicate minerals and melts (e.g., Holycross et al. 2018).

4.2 Modeling

Core-to-rim decreases in the Li content of Martian clinopyroxenes have previously been interpreted to reflect the loss of Li from cpx to an exsolved fluid phase. Our new mineral-melt partition coefficients offer the opportunity to evaluate this model and determine if normal igneous differentiation (i.e., cooling and

crystallization) could have produced the observed reverse zoning patterns. Although reverse zoning of the LLEs has been measured in many different types of Martian meteorites, we focus our modeling efforts on reproducing the crystallization conditions of cpx in the Shergotty meteorite. The equilibrium phase assemblage experiments of Dann et al. (2001) suggest the high-Li pigeonite cpx cores of the Shergotty meteorite will crystallize from melt in the Martian mantle starting at 1175 °C, with low-Li augite rims precipitating starting at 1075 °C. Clinopyroxene is the liquidus phase and sole phase crystallized until plagioclase comes in at 1075 °C. We used the experiments Dann et al. (2001) to quantify changes in the mode of cpx during cooling from 1190 °C (only melt) to 1075 °C (44 mode% cpx):

$$S\text{hergotty cpx mode } (\%) = -0.3588T + 425.56 \quad (4)$$

where *T* is temperature in degrees Celsius.

Our preliminary results suggest the compatibility of Li in Martian cpx will decrease as pressure and temperature decrease. We parameterized $D_{Li}^{cpx/melt}$ as a function of temperature for Mix 2 with a linear regression:

$$log D_{Li,mix\,2}^{cpx/melt} = 0.0073T - 9.1533 \quad (5)$$

where *T* is temperature in degrees Celsius.

We examined the change in the Li content of cpx crystallizing from the Shergotty source melt as a function of cpx mode during equilibrium crystallization using the following equation:

$$\frac{C_R}{C_0} = \mathrm{D}/[\mathrm{D} + \mathrm{F}(1 - \mathrm{D})] \ (6)$$

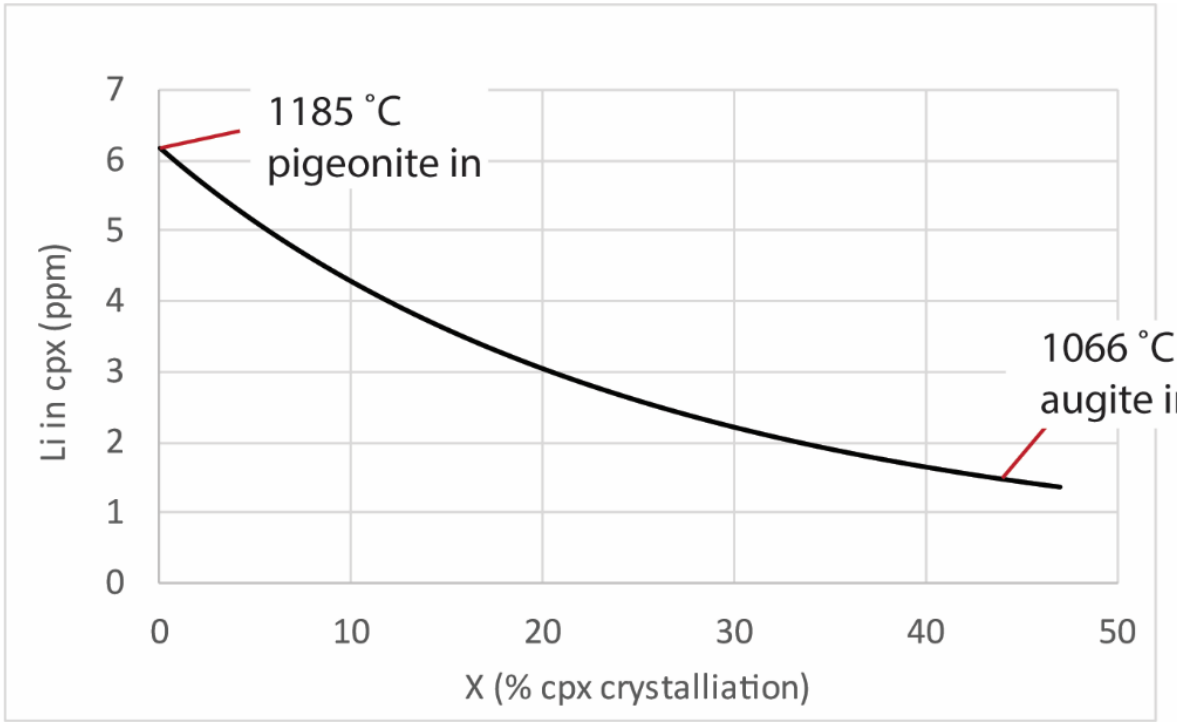

Figure 12: Equilibrium crystallization model for Li in cpx as a function of % cpx crystallized

where C_R is the concentration of Li in the crystallizing cpx, C_0 is the initial concentration of Li in the melt, *F* is the fraction of melt remaining, and *D* is the cpx/melt partition coefficient for Li. We used equations 4 and 5 to recalculate $D_{Li}^{cpx/melt}$ at each crystallization step for input into equation 6. Estimates of bulk Li in Shergotty range from ~4-6 ppm (Lentz et al. 2001). Use of these values (e.g., 6 ppm) for C_0 in our equilibrium crystallization model results in Li concentrations in cpx cores that are well below observed values (Li in Shergotty cores reaches up to 8 ppm; e.g., McSween et al. 2001, Lentz et al. 2001, Udry et al. 2016). This raises the following possibilities: 1) that Li is more compatible in cpx at the conditions of the Martian mantle than measured; 2) that Li was lost from the Martian mantle to an exsolved fluid

phase during igneous evolution or later low-temperature alteration of the Shergotty meteorite; 3) that estimates of the bulk Li in Shergotty are possibly erroneous. Regardless, we find that a value of C_0=20 ppm is sufficient to reproduce the Li concentrations in Shergotty cpx cores.

Our equilibrium crystallization model suggests that the concentration of Li in cpx will decrease as crystallization progresses during cooling (Figure 12). This is a result of the positive relationship between T and $D_{Li}^{cpx/melt}$ in our Martian composition experiments (e.g., equation 5). Although Li is incompatible in cpx at all conditions of our model, it becomes more incompatible at the lower temperature conditions of augite crystallization. Consequently, even though the concentration of Li in the melt is increasing as crystallization progresses, this increase is not reflected in the Li composition of the newly crystallized cpx, as would be expected if the Li partition coefficient was independent of temperature. This suggests that the reverse zoning of Li in Shergotty cpx could be the result of simple crystallization and cooling, rather than the loss of Li to a fluid phase between the precipitation of pigeonite and augite.

We compare the results of our model to the observations of Lentz et al. (2001) in Figure 13. Previous studies have plotted the Li content of cpx vs TiO_2 content to examine variations in incompatible element concentration in cpx during crystallization. We parameterize the partitioning of TiO_2 between cpx and melt in Mix 2 with the following equation:

$$D_{TiO_2,mix\,2}^{cpx/melt} = -0.0004T - 0.5991 \quad (7)$$

where T is temperature in degrees Celsius. We used this relationship to examine the TiO_2 content of cpx crystallizing from the Shergotty source melt as a function of cpx mode during equilibrium crystallization using equation 6. We used a TiO_2 (C_0) value for the Shergotty melt of 2.6 wt%. Our crystallization model does not produce the

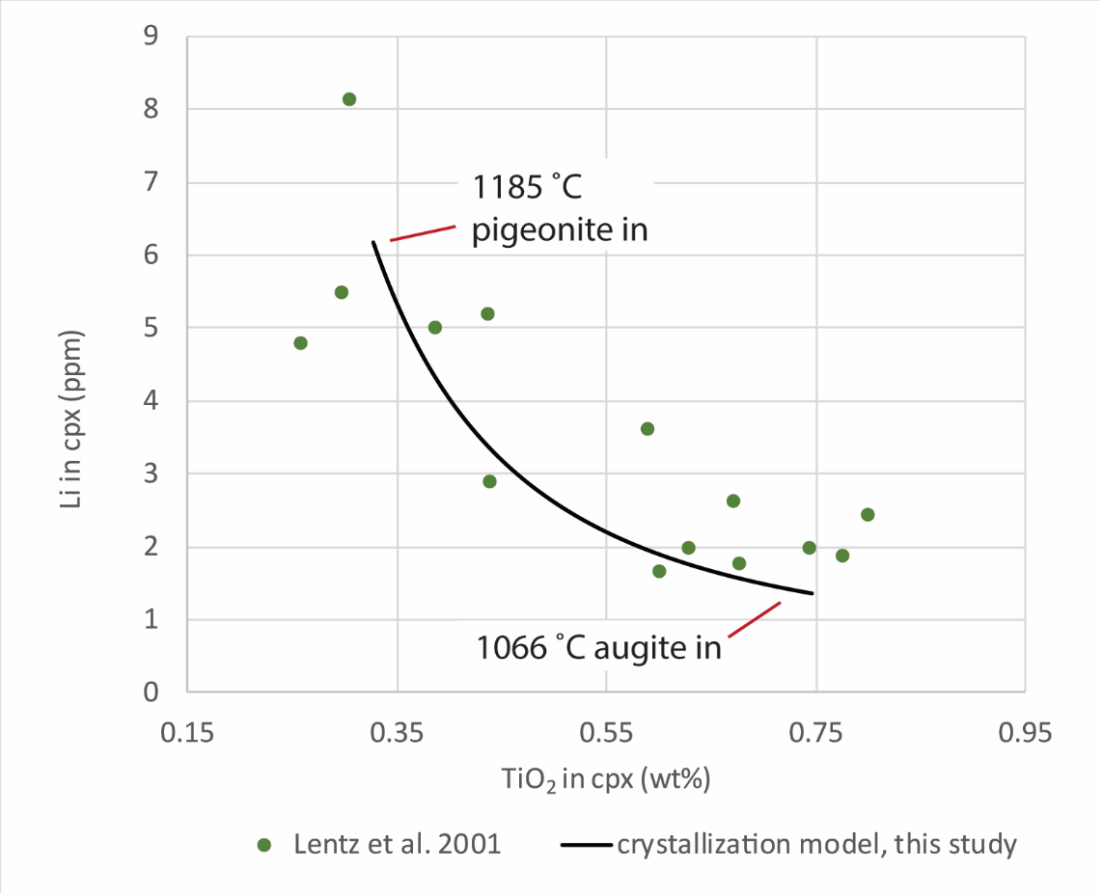

Figure 13: Li in cpx (ppm) versus TiO_2 in cpx (wt%)

TiO_2 values of the Shergotty cpx cores with lower C_0 values.

We compare the Li and TiO_2 contents of our modeled Shergotty cpx with measurements of Shergotty cpx from Lentz et al. (2001) in Figure 13. We find our equilibrium crystallization model produces cpx compositions that overlaps quite well

with observations, suggesting that changes in the compatibility of Li in cpx during cooling may be in part responsible for driving LLE reverse zoning in Martian cpx.

CONCLUSIONS

We find that the partitioning of Li between cpx and melt varies as a function of pressure and temperature and is not strongly impacted by cpx or bulk composition. Our preliminary data show $D_{Li}^{cpx/melt}$ for the Martian composition decreases during cooling and decompression. Consequently, the Li reverse zoning patterns found in Martian cpx may be the result of regular igneous differentiation processes . This casts doubt on the hypothesis that Li concentration profiles in Martian cpx record the loss of Li to a fluid or vapor phase during degassing.

However, controls on Li partitioning are still not well understood and further experiments conducted at systematically varied temperatures and pressures should be executed to determine how Li partitions between minerals, melts, and fluids to substantiate the trends we see in this study.

REFERENCES

Barrat, J. A., et al. "Petrology and chemistry of the picritic shergottite North West Africa 1068 (NWA 1068)." *Geochimica et Cosmochimica Acta* 66.19 (2002): 3505-3518.

Beck, Pierre, et al. "Li isotopic variations in single pyroxenes from the Northwest Africa 480 shergottite (NWA 480): a record of degassing of Martian magmas?." *Geochimica et Cosmochimica Acta* 68.13 (2004): 2925-2933.

Beck, P., et al. "Li isotopic composition of the NWA 480 Shergottite." *Lunar and Planetary Science Conference*. 2004.

Berlo, Kim, et al. "Geochemical precursors to volcanic activity at Mount St. Helens, USA." *Science* 306.5699 (2004): 1167-1169.

Blundy, J. D., et al. "Sodium partitioning between clinopyroxene and silicate melts." *Journal of Geophysical Research: Solid Earth* 100.B8 (1995): 15501-15515.

Blundy, J. D., J. A. C. Robinson, and B. J. Wood. "Heavy REE are compatible in clinopyroxene on the spinel lherzolite solidus." *Earth and Planetary Science Letters* 160.3-4 (1998): 493-504.

Brenan, J. M., et al. "Behaviour of boron, beryllium, and lithium during melting and crystallization: constraints from mineral-melt partitioning experiments." *Geochimica et Cosmochimica Acta* 62.12 (1998): 2129-2141.

Brenan, James M., Frederick J. Ryerson, and Henry F. Shaw. "The role of aqueous fluids in the slab-to-mantle transfer of boron, beryllium, and lithium during subduction: experiments and models." *Geochimica et Cosmochimica Acta* 62.19-20 (1998): 3337-3347.

Dann, J. C., et al. "Phase equilibria of the Shergotty meteorite: Constraints on pre-eruptive water contents of Martian magmas and fractional crystallization under hydrous conditions." *Meteoritics & Planetary Science* 36.6 (2001): 793-806.

Edmonds, Marie. "Partitioning of light lithophile elements during basalt eruptions on Earth and application to Martian shergottites." *Earth and Planetary Science Letters* 411 (2015): 142-150.

Giuffrida, Marisa, and Marco Viccaro. "Three years (2011–2013) of eruptive activity at Mt. Etna: Working modes and timescales of the modern volcano plumbing system from micro-analytical studies of crystals." *Earth-Science Reviews* 171 (2017): 289-322.

Herd, Christopher DK, et al. "The behavior of Li and B during planetary basalt crystallization." *American Mineralogist* 89.5-6 (2004): 832-840.

Herd, Christopher DK, et al. "Light lithophile elements in martian basalts: Evaluating the evidence for magmatic water degassing." *Geochimica et Cosmochimica Acta* 69.9 (2005): 2431-2440.

Hervig, Richard L., et al. "Isotopic and elemental partitioning of boron between hydrous fluid and silicate melt." *American Mineralogist* 87.5-6 (2002): 769-774.

Holycross, M. E., et al. "Diffusive fractionation of Li isotopes in wet, highly silicic melts." *Geochemical Perspectives Letters* 6 (2018): 39-42.

Iveson, Alexander A., et al. "Fluid-melt trace-element partitioning behaviour between evolved melts and aqueous fluids: Experimental constraints on the magmatic-hydrothermal transport of metals." *Chemical Geology* 516 (2019): 18-41.

Kent, Adam JR, et al. "Vapor transfer prior to the October 2004 eruption of Mount St. Helens, Washington." *Geology* 35.3 (2007): 231-234.

Khitarov, N. I., A. A. Kadik, and E. B. Lebedev. "Solubility of water in a basalt melt." *Geokhimia* 7 (1968): 763-772.

Lentz, R. C. F., et al. "Water in martian magmas: clues from light lithophile elements in shergottite and nakhlite pyroxenes." *Geochimica et Cosmochimica Acta* 65.24 (2001): 4551-4565.

Marschall, Horst R., et al. "The boron and lithium isotopic composition of mid-ocean ridge basalts and the mantle." *Geochimica et Cosmochimica Acta* 207 (2017): 102-138.

McDade, Paula, Jon D. Blundy, and Bernard J. Wood. "Trace element partitioning on the Tinaquillo Lherzolite solidus at 1.5 GPa." *Physics of the Earth and Planetary Interiors* 139.1-2 (2003): 129-147.

McSween Jr, Harry Y., et al. "Geochemical evidence for magmatic water within Mars from pyroxenes in the Shergotty meteorite." *Nature* 409.6819 (2001): 487-490.

Neukampf, Julia, et al. "Time scales of syneruptive volatile loss in silicic magmas quantified by Li isotopes." *Geology* 49.2 (2021): 125-129.

Ottolini, Luisa, et al. "New experimental determination of Li and B partition coefficients during upper mantle partial melting." *Contributions to Mineralogy and Petrology* 157 (2009): 313-325.

Rollinson, Hugh, and Victoria Pease. *Using Geochemical Data: To Understand Geological Processes*. 2nd ed. Cambridge: Cambridge UP, 2021. Print.

Ryan, Jeffrey Gerard. *The systematics of lithium, beryllium and boron in young volcanic rocks*. Columbia University, 1989.

Shannon, Robert D. "Revised effective ionic radii and systematic studies of interatomic distances in halides and chalcogenides." *Acta crystallographica section A: crystal physics, diffraction, theoretical and general crystallography* 32.5 (1976): 751-767.

Seyfried Jr, W. E., D. R. Janecky, and M. J. Mottl. "Alteration of the oceanic crust: implications for geochemical cycles of lithium and boron." *Geochimica et Cosmochimica Acta* 48.3 (1984): 557-569.

Udry, Arya, et al. "Lithium isotopes and light lithophile element abundances in shergottites: Evidence for both magmatic degassing and subsolidus diffusion." *Meteoritics & Planetary Science* 51.1 (2016): 80-104.

Webster, J. D., J. R. Holloway, and R. L. Hervig. "Partitioning of lithophile trace elements between H 2 O and H 2 O+ CO 2 fluids and topaz rhyolite melt." *Economic Geology* 84.1 (1989): 116-134.